01 Sep 2003

Utilization of a Piezoelectric Polymer to Sense Harmonics of Electromagnetic Torque

Jason Neely

Steven Pekarek
Missouri University of Science and Technology

Daniel S. Stutts
Missouri University of Science and Technology, stutts@mst.edu

Philip Beccue

Recommended Citation

J. Neely et al., "Utilization of a Piezoelectric Polymer to Sense Harmonics of Electromagnetic Torque," *Power Electronics Letters*, Institute of Electrical and Electronics Engineers (IEEE), Sep 2003.
The definitive version is available at https://doi.org/10.1109/LPEL.2003.822547

Utilization of a Piezoelectric Polymer to Sense Harmonics of Electromagnetic Torque

P. Beccue, J. Neely, S. Pekarek, and D. Stutts

***Abstract*—In this paper, the use of a piezoelectric polymer material to measure the harmonics of electromagnetic torque produced by a permanent magnet synchronous machine is described. The advantages of the polymer include low cost, durability, and flexibility. In addition, wide-bandwidth sensors are relatively easy to design and couple to drive system hardware for harmonic evaluation or to use in feedback-based control. To illustrate the use of the polymer, the electrical and mechanical properties of three sensors are described. The results of time-domain simulation and hardware experiments are used to validate that the voltage obtained from the sensors is linearly related to the torque ripple produced by the machine.**

***Index Terms*—Permanent magnet machine, piezoelectric materials, torque measurement.**

I. Introduction

In NUMEROUS applications, vibration or acoustic noise that results from harmonics in the electromagnetic torque produced by electric machines is a design issue. Methods of measuring torque harmonics have been documented in [1]–[4]. In [1], an inline torque transducer that uses surface acoustic wave technology to sense twisting of the shaft is used to measure torque ripple harmonics. In [2], a strain gauge bridge is used as a torque sensor; however, the average electromagnetic torque is balanced by a constant load (a flywheel with a large inertia) to ensure that average torque is not measured by the sensor. Since average torque is not included, the accuracy of the measured torque ripple is increased. In another technique described in [2], current sensors are used to predict relative amplitudes of torque ripple based upon the ripple component of the sum of the square of the stator phase currents. In [3], a high-precision position encoder is used to calculate torque using an observer algorithm. In [4], disturbances in a motor housing that result from torque harmonics produced by a permanent magnet synchronous machine (PMSM) are measured using an accelerometer and/or microphone.

Although previous methods are effective as a diagnostic tool or for use in custom drive applications, developing low-cost practical techniques for sensing torque ripple that can be incorporated in mass-produced drives is an area of active research. Toward this objective, a piezoelectric polymer material has been investigated to measure the harmonics of electromagnetic torque produced by a PMSM. In this paper, the properties of the polymer that are important for sensor construction are first described. The design and installation of three sensors (including mechanical and thermal constraints) is then presented. Results of time-domain simulation and hardware experiments are used to demonstrate that the voltage obtained from the sensors is linearly related to torque ripple amplitude.

Manuscript received August 28, 2003. This work was supported by the National Science Foundation under Grant 01 202 531. Recommended by Associate Editor D. Perreault.

P. Beccue and S. Pekarek are with the Department of Electrical Engineering University of Missouri-Rolla, Rolla, MO 65409 USA.

J. Neely is with the Sandia National Labs, Albuquerque, NM 87123 USA.

D. Stutts is with the Department of Mechanical Engineering, University of Missouri-Rolla, Rolla, MO 65409 USA.

Digital Object Identifier 10.1109/LPEL.2003.822547

II. Piezoelectric Materials

In general, piezoelectric materials produce an electric charge in response to mechanical stress. Conversely, an applied electric field will induce strain and concomitant stress in a piezoelectric material, which allows the use of piezoelectric materials for actuation [5]. The "piezoelectric effect" was discovered in quartz by brothers J. and P. Curie in 1880. Since then, numerous materials have been produced that exhibit piezoelectric behavior. The materials are typically grouped into categories of ceramics and polymers. Commonly known piezoelectric ceramics include lead zirconate titanate (PZT) and lead lanthanum zirconate titanate (PLZT). The most common piezoelectric polymer is polyvinylidene fluoride (PVDF). Properties of PZT and PVDF that are important for sensor design are shown in Table I [6]. Although shown for a single ceramic and polymer, the values provided in Table I are representative of a broad class of materials within their respective categories.

In Table I, the material properties listed include density, relative permittivity, piezoelectric strain constants, and piezoelectric stress constants. The stress constants reflect the ability of a material to convert applied stress into electric potential. The strain constants define the ability of a material to convert applied voltage into mechanical displacement. It is noted that each material has multiple values for the stress and strain constants. Subscripts are used to define the direction of the electric field versus the direction of mechanical displacement. A diagram depicting axes on a piezoelectric element is shown in Fig. 1.

From Table I, it can be seen that the stress constants of PVDF are much greater than those of PZT. Therefore, for elements of equal dimension under identical pressure, PVDF produces a greater voltage than PZT. In contrast, the strain constants of PZT are much larger than those of PVDF. Therefore, for elements of equal dimension that are excited by an identical source voltage, PZT produces a greater displacement than PVDF. For sensing torque ripple, the stress constants are more significant. Comparing stress constants, it is clear that PVDF requires a smaller sensor to obtain a given voltage.

Loosely defined, Young's modulus represents the force needed to elongate (or compress) the material. By comparing

TABLE I
PIEZOELECTRIC MATERIAL PROPERTIES

Property		Units	PVDF (polymer)	PZT (ceramic)
Density		$10^{3}\ \frac{\text{kg}}{\text{m}^3}$	1.78	7.6
Relative Permittivity		$\frac{\varepsilon}{\varepsilon_o}$	12	1200
Piezoelectric Strain Constant	d_{31}	$10^{-12}\ \frac{\text{m}}{\text{V}}$	23	180
	d_{33}	$10^{-12}\ \frac{\text{m}}{\text{V}}$	33	360
Piezoelectric Stress Constant	g_{31}	$10^{-3}\ \frac{\text{V/m}}{\text{N/m}^2}$	220	10
	g_{33}	$10^{-3}\ \frac{\text{V/m}}{\text{N/m}^2}$	330	18
Young's (Elastic) Modulus		$10^{10}\ \frac{\text{N}}{\text{m}^2}$	0.3	4.9

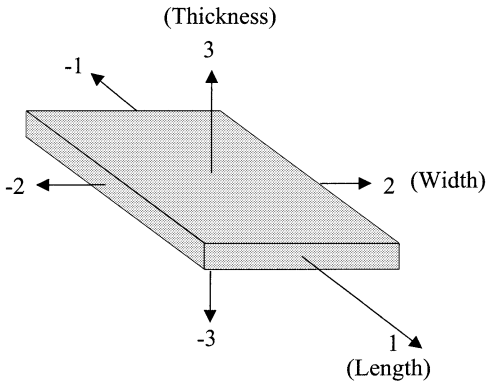

Fig. 1. Defined axis of the piezoelectric material.

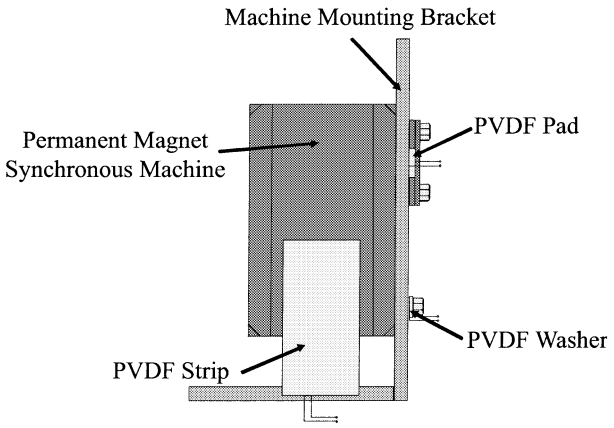

Fig. 2. Mounting configuration for the three sensors.

values of Young's Modulus, it is clear that PVDF is more easily compressed than PZT. PVDF is also more compliant, allowing one to sense stress applied in the *1* axis of the material. In contrast, the stiffness of PZT limits the force that can be applied along the *1* axis before the material breaks.

III. TORQUE RIPPLE SENSORS

Three methods of creating torque ripple sensors using PVDF have been considered. These include using the material as a thin film strip, pad, and washer. The mounting configurations of each are shown in Fig. 2. The strip is mounted between the motor housing and the motor mount. The pad is placed between the motor mount and a small bracket that is bolted to the motor housing. The washer is placed on a bolt used to attach the motor to the mount. In the pad and washer configurations, the piezo material produces voltage in response to vibrations in the motor housing, which creates stress along the *3* axis of the material. In the strip configuration, voltage is produced in response to rotational movement of the stator housing with respect to a fixed point on the mount. Therein, stress is placed in the *1* axis of the material.

Provided the material does not reach a mechanical resonance (described in the Section IV), the relationship between stress and voltage is linear in each configuration, and can be expressed in a form [6]

$$v_s(f) = g_{3n}\,\mathrm{st}_n(f)h \tag{1}$$

where g_{3n} is the stress constant of the n axis, st_n is the applied mechanical stress in the n axis, h is the thickness of the material. Stress is expressed as a function of frequency (f) to denote the fact that the influence of torque harmonics on the mount system is frequency dependent. The dynamic range over which the material translates stress into a voltage is between 0.001 Hz and 10^9 Hz [6]. In all three configurations, the PVDF is coated on each side with silver ink, producing a conductive layer on which to measure induced voltage.

Since the sensors are produced by coating both sides of the polymer with a conducting material, they can be modeled electrically as a time-varying voltage source and a series source capacitance as shown in Fig. 3 [6]. The value of capacitance is

$$C_s = \varepsilon\frac{A}{h} \tag{2}$$

where ε is the dielectric constant of the piezoelectric material and A is the area of the conducting material.

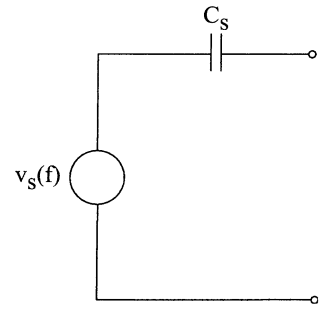

Fig. 3. Equivalent circuit of the film.

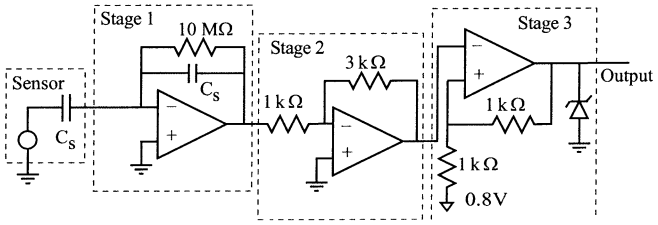

Fig. 4. Amplifier from sensor to processor input.

The series capacitance acts as a high-pass filter for the sensors. The ability to capture low frequency signals is limited without the use of external circuit components. In practice, an external circuit is used to perform amplification and signal conditioning. One example of a circuit that is used in a feedback control loop is shown in Fig. 4. Therein, a three-stage op-amp circuit is placed between the sensor and the analog input to a processor board. The first stage of the amplifier is designed to effectively cancel the series capacitance of the sensor [7], the second stage is used to provide gain, and the third stage is designed to add offset and to limit the voltage so that the input to the processor is between 0 and 3.3 V. Two LF353 op-amp chips were used to construct the circuit shown in Fig. 4. Component values are shown for the strip sensor.

The cost of a strip of PVDF with a 28-μm thickness is on the order of 0.1 U.S.$/cm^2. Cost increases with material thickness. The washer and pad have a material thickness of 100 μm and cost roughly an order of magnitude more than the 28 μm strip of the same area.

IV. Mechanical Limits

The equivalent circuit of a piezoelectric element shown in Fig. 3 becomes inaccurate as the frequency of the torque harmonics approach the natural resonant frequency of the material. The natural frequencies of the pad and washer can be predicted using finite strain theory [8], [9]. Specifically, applying Newton's second law and using the mechanical constitutive model, the displacement of the pad and washer in the *3* axis is expressed as a function of position and time as

$$\rho A \frac{\partial^2 u}{\partial t^2} = A Y^D \left(1 + \frac{\partial u}{\partial x}\right) \frac{\partial^2 u}{\partial x^2} \tag{3}$$

where x is the position along the *3* axis, u is the displacement in the *3* axis as a function of x and t, A is the cross-sectional area of the sensor, ρ is the mass density of the material, and Y^D is Young's modulus under constant electric displacement.

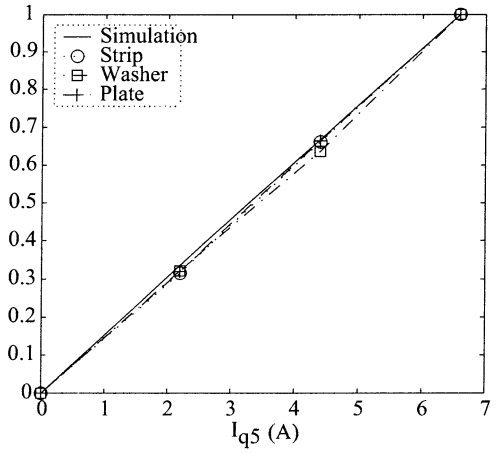

Fig. 5. Comparison of measured voltage and simulated 6th harmonic torque ripple for strip, pad, and washer sensors.

Using one-dimensional finite strain theory and assuming $Y^D A \gg F_o$, where F_o is the preload force, the derivative of u with respect to x at equilibrium may be expressed as

$$\frac{\partial \bar{u}}{\partial x} = \frac{F_o}{Y^D A}. \tag{4}$$

where the overbar denotes the constant average strain due to the preload. Substituting (4) into (3), the finite strain, one-dimensional wave equation linearized about the equilibrium strain may be written as

$$\frac{\partial^2 u}{\partial t^2} = c^2 \frac{\partial^2 u}{\partial x^2} \tag{5}$$

where

$$c = \sqrt{\left(1 + \frac{F_o}{Y^D A}\right) \frac{Y^D}{\rho}} \tag{6}$$

denotes the linear wave speed incorporating the effects of the static preload. Solving (5) (using displacement as the boundary conditions), the natural resonant frequencies (in Hertz) of the pad and washer sensors under a preload force are approximated as

$$f_n = \frac{n}{2h} \sqrt{\frac{Y^D \left(1 + \frac{F_o}{Y^D A}\right)}{\rho}} \tag{7}$$

where n is the mode number. From (7), it can be seen that a compressive (negative) preload will lower the resonant frequencies. For the washer and pad configurations shown in Fig. 2, the lowest resonant frequency is on the order of 10^7 Hz for an applied force on the order of 10^2 N.

The resonant frequencies of the strip sensor under tension may also be approximated in closed form. Assuming the strip sensor behaves essentially like a string under tension, the natural frequencies of the strip may be approximated using linear string theory [10]

$$f_n = \frac{n}{2L} \sqrt{\frac{T_o}{\rho A}} \tag{8}$$

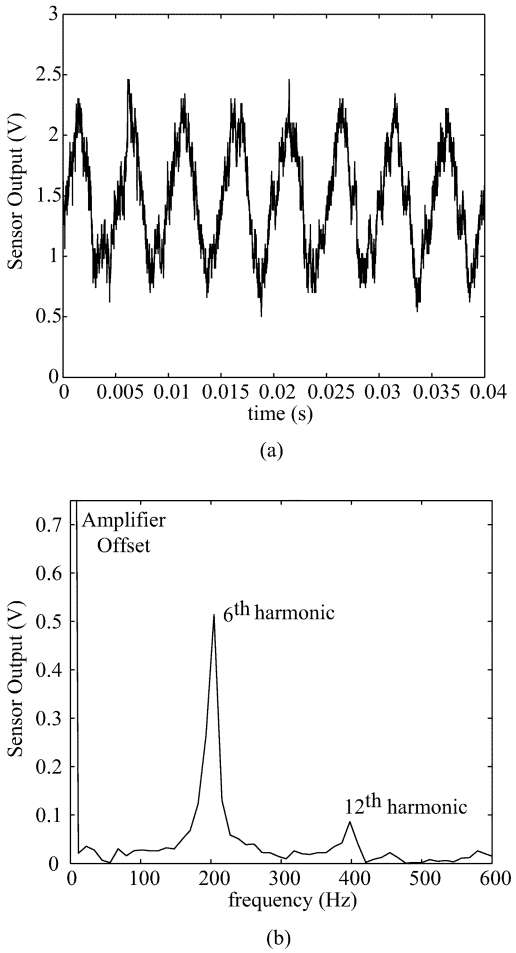

Fig. 6. Signals of pad sensor at 333 rpm (measured at output of amplifier circuit). (a) Time. (b) Frequency-domain.

where T_o is the tension in the strip and L is the length of the strip. For the strip configurations shown in Fig. 2, the lowest resonant frequency is on the order of 10^4 Hz for an applied force on the order of 10^2 N.

In addition to considering mechanical resonance, care must be given to prevent an excessive load on the sensor. A load exceeding 50 MPa will cause the material to depole. Thus it no longer acts as a stress/voltage transducer. For PZT, the average depoling load is 80 MPa. Thermal effects must also be considered. In general, the stress constants of the piezoelectric material increase with temperature [11]. However, PVDF will depole as temperatures reach 90 °C. PZT will depole as temperatures reach 300 °C.

V. Sensor Validation and Performance

The voltage produced by each of the sensors has been measured to determine if the signal is proportional to the torque ripple produced by a PMSM. The machine studied is designed using three full-pitch concentrated stator phase windings (one slot/pole/phase) that are wye-connected. The fundamental torque harmonic occurs at the 6th order of rotor electrical angular velocity. A second harmonic occurs at the 12th order of rotor electrical angular velocity. In the study, the rotor position and stator current harmonics are controlled such

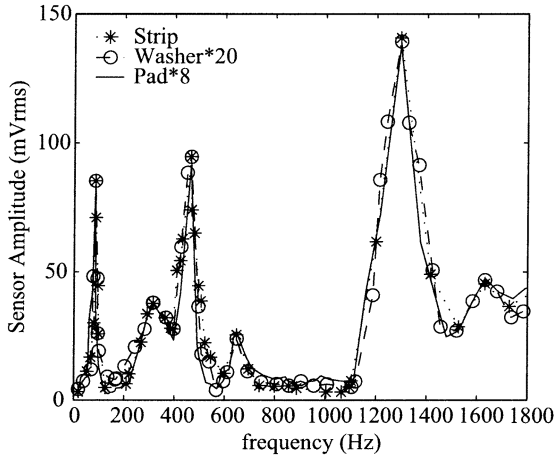

Fig. 7. Frequency response of the three sensors.

that the magnitude of the 6th harmonic torque can be expressed as [12]

$$T_{e6} = \frac{3P}{4}[(\kappa_{e5} + \kappa_{e7})\kappa_{iq1} + (\kappa_{e1} + \kappa_{e11})\kappa_{iq5}] + T_{\text{cog6}}. \quad (9)$$

The values $\kappa_{e1}, \kappa_{e5}, \kappa_{e7}$, and κ_{e11} represent magnitudes of the 1st, 5th, 7th, and 11th harmonics of back-electromotive force, respectively; κ_{iq1} and κ_{iq5} are the magnitudes of the 1st and 5th harmonics of stator current; and P is the number of poles. The variable T_{cog6} represents the amplitude of the 6th harmonic of cogging torque that results from the interaction of the rotor magnets with the stator teeth. To test the torque ripple sensors, the fundamental component of stator current was held constant at 16.5 A and the 5th current harmonic was increased from 0 to 6.6 A. The voltage obtained from the sensors, measured at the input to the amplifier circuit shown in Fig. 4, is plotted in Fig. 5.

To generate the plot, the voltage and torque ripple amplitudes at $\kappa_{iq5} = 0$ A have been subtracted from subsequent values and the results normalized to the $\kappa_{i5} = 6.6$ A value. Also shown in Fig. 5 are the expected torque ripple amplitudes obtained by measuring the respective back-emf components and cogging torque, plugging values into (9), and normalizing the results to the maximum ($\kappa_{i5} = 6.6$ A) amplitude. Comparing plots, it can be seen that there is a linear correlation between the measured voltage and the predicted 6th harmonic of the torque ripple in all three sensor configurations.

A time-domain signal of the voltage from the pad sensor is shown in Fig. 6(a). To obtain this response, the voltage was measured at the output of the circuit shown in Fig. 4. A dc offset exists to ensure the voltage is always between 0 and 3.3 V for the processor used in a feedback control loop. Nevertheless, from the plot, it can be seen that the signal contains a strong 6th harmonic content. Although difficult to notice in the time-domain plot, a 12th harmonic is also present. It is noted that a high-frequency component is observed in the time-domain plot. This component is not the result of electrical noise. Rather, it is the measurement of vibrations that result from switching harmonics in the stator currents. A frequency domain plot of the voltage is shown in Fig. 6(b). Therein, vibrations due to the dominant 6th harmonic torque ripple and the 12th harmonic torque ripple are clearly observed.

TABLE II
SENSOR PROPERTIES

Properties		Strip	Washer	Pad
Physical Dimensions	Length {outer radius} (cm)	17.1	{1.27}	2.54
	Width {inner radius} (cm)	2.18	{0.25}	2.54
	Thickness (cm)	0.005	0.102	0.102
Capacitance (pF)		5420	99.3	109
Signal-to-Noise (dB)		49	39	40
Baseline noise (mV_{rms})		1.4	2.1	2.3

The frequency response of each sensor was measured (for the given mount configuration) by running the motor under open-circuit conditions at rotor speeds of 30–3000 RPM. The frequency of the 6th torque ripple harmonic for the given range of rotor speed varies from 18 to 1800 Hz. Voltages were measured at the terminals of the sensors and are plotted in Fig. 7. The amplitudes of the washer and pad are scaled to allow plotting on the same axis as the strip. From Fig. 7, it is seen that the output voltage amplitude of the sensors is a function of frequency. This is expected, since the sensors detect strain that results from torque ripple harmonics. Although the cogging torque amplitude is identical at each frequency, the response of the mount is dependent upon frequency. It is important to note that although the three sensors produce different amplitude voltages at a given frequency, the three sensors have a nearly identical frequency response. The physical size, capacitance, signal-to-noise ratio, and baseline noise of each sensor is listed in Table II. The signal-to-noise ratios (SNRs) were calculated using data obtained by simultaneously measuring a sensor voltage (at the output of the amplifier circuit) on all four channels of an oscilloscope with the PMSM driven at 333 rpm. At the given rotor speed, a 6th torque ripple harmonic is present at 200 Hz. From Fig. 7, it is seen that this results in relatively small amplitude of sensor voltage. To establish the value of the sensor signal, the voltages obtained at the four channels were summed and then divided by four. The baseline noise was calculated by subtracting the resulting sensor signal from one of the four channels. The SNR was then calculated using the rms values of the signal and noise. Comparing values, it is seen that the strip sensor had the largest SNR. This is expected, since the output voltage of the strip was significantly larger than the pad or washer.

It is noted that each of the sensors has high internal impedance, which can lead to noise susceptibility. In testing of the sensors under different hardware and mount configurations, no distinct difference between the three configurations has been found. As the sensors have been tested using different hardware and mount configurations, there have been infrequent instances in which noise has corrupted sensor signals. In these instances, the noise has been eliminated by shielding the cable and terminating one end of the shield to ground.

The sensitivity of three sensors has been tested by varying the 5th harmonic of stator current to minimize the 6th torque ripple harmonic using a torque control strategy described in [13]. Reasonable SNR (>20 dB) have been obtained from each sensor for torque ripple amplitudes as low as 10 mNm. Accurately controlling the amplitude of torque ripple to values below 10 mNm to establish precise bounds on sensitivity (for the given application) has been a challenge and remains the topic of ongoing investigation.

VI. CONCLUSION

Three sensors have been developed using a polymer piezoelectric material PVDF. As a sensor, PVDF has several advantages over PZT, including higher stress constants, higher compressibility, and greater flexibility. The sensors are relatively low in cost and have a high durability, making them an ideal candidate for feedback-based control of torque ripple harmonics in electric machines.

REFERENCES

[1] A. Wu and P. Chapman, "Cancellation of torque ripple due to nonidealities of permanent magnet synchronous machine drives," in *Proc. IEEE Power Electronics Specialist Conf.*, 2003, pp. 256–261.
[2] L. Sun, H. Gao, Q. Song, and J. Nei, "Measurement of torque ripple in pm brushless motors," in *Proc. IEEE Industry Applications Conf.*, 2002, pp. 2567–2571.
[3] S. Kang and S. Sul, "Direct torque control of the brushless dc motor with nonideal trapezoidal back emf," in *Proc. IEEE Applied Power Electronics Conf.*, 1995, pp. 392–398.
[4] T. Su, S. Hattori, M. Ishida, and T. Hori, "Suppression control method for torque vibration of ac motor utilizing repetitive controller with Fourier Transform," *IEEE Trans. Ind. Applicat.*, vol. 38, pp. 1316–1325, Sept./Oct. 2002.
[5] J. R. Friend and D. S. Stutts, "The dynamics of an annular piezoelectric motor stator," *J. Sound Vibr.*, vol. 203–204, pp. 421–437, 1997.
[6] *Piezo Film Sensors Technical Manual*, 1999. pp. 2–16.
[7] T. Janiczek, "Analysis of PVDF transducer signals stimulated by mechanical tension," *J. Electros.*, vol. 51–52, pp. 167–172, 2001.
[8] G. A. Maugin, *Nonlinear Electromechanical Effects and Applications*. Singapore: World Scientific, 1985, pp. 41–68.
[9] I. S. Sokolnikoff, *Mathematical Theory of Elasticity*, 2nd ed. New York: McGraw-Hill, 1956, pp. 29–59.
[10] S. Rao, *Mechanical Vibrations*, 4th ed. Englewood Cliffs, NJ: Prentice-Hall, 2004, ch. 8.
[11] A. Salimi and A. A. Yousefi, "FTIR studies of β-phase crystal formation in stretched PVDF films," *Polymer Testing*, vol. 22, pp. 699–704, 2003.
[12] P. Beccue, S. Pekarek, J. Neely, and D. Stutts, "Design of a closed-loop controller for mitigation of torque ripple in a brushless DC machine," in *Proc. IEEE Power Electronics Specialist Conf.*, 2003, pp. 1664–1670.
[13] P. L. Chapman, S. D. Sudhoff, and C. A. Whitcomb, "Optimal current control strategies for surface-mounted permanent-magnet synchronous machine drives," *IEEE Trans. Energy Conversion*, vol. 14, pp. 1043–1050, Dec. 1999.